

**Flexible and highly conductive AgNWs/PEDOT:PSS functionalized
aramid non-woven fabric for high-performance electromagnetic
interference shielding and Joule heating**

Lele Li ^a, Baojie Sun ^a, Wenyue Li ^a, Liang Jiang ^a, Yanfen Zhou ^{a*}, Jianwei Ma ^a,
Shaojuan Chen ^b, Xin Ning ^a, Feng-Lei Zhou ^{a, c*}

^a Industrial Research Institute of Nonwovens and Technical Textiles, Shandong Center
for Engineered Nonwovens, College of Textiles and Clothing, Qingdao University,
Qingdao, 266071, P. R. China

^b Eco-Textile Collaborative Innovation Center, College of Textiles and Clothing,
Qingdao University, Qingdao, 266071, P. R. China

^c Centre for Medical Image Computing, University College London, London, WC1V
6LJ, UK

* Corresponding author: yanfen.zhou@qdu.edu.cn (Yanfen Zhou),
fenglei.zhou@ucl.ac.uk (Feng-Lei Zhou)

Abstract: High-performance multifunctional textiles are highly demanded for human health-related applications. In this work, a highly conductive nonwoven fabric was fabricated by coating silver nanowires (AgNWs)/poly(3,4-ethylenedioxythiophene):poly(styrenesulfonate) (PEDOT:PSS) on a commercial poly(m-phenylene isophthalamide) (PMIA) nonwoven fabric through a multi-step dip coating process. The as-prepared PMIA/AgNWs/PEDOT:PSS composite nonwoven fabric showed an electrical resistance as low as $0.92 \pm 0.06 \Omega/\text{sq}$ with good flexibility. The incorporation of the PEDOT:PSS coating layer improved the adhesion between AgNWs and PMIA nonwoven fabric, and also enhanced the thermal stability of the composite nonwoven fabric. Electromagnetic interference (EMI) shielding and Joule heating performances of the PMIA/AgNWs/PEDOT:PSS composite nonwoven fabric were also investigated. The results showed that the average EMI shielding effectiveness (SE) of the single-layer nonwoven fabric in X-band was as high as 56.6 dB and retained a satisfactory level of SE after being washed, bended and treated with acid/alkali solution and various organic solvents. The composite nonwoven fabric also exhibited low voltage-driven Joule heating performance with reliable heating stability and repeatability. It can be envisaged that the multifunctional PMIA/AgNWs/PEDOT:PSS nonwoven fabric with reliable stability and chemical robustness could be used in EMI shielding devices and personal thermal management products.

Keywords: Nonwoven fabric; Silver nanowires; PEDOT:PSS; Electromagnetic shielding; Joule heating

1. Introduction

With the arrival of 5G communication era, the introduction of high frequencies, the upgrading of hardware components and the increase in the number of networked devices have caused increasingly serious electromagnetic interference and

electromagnetic radiation [1, 2]. Meanwhile, with the emerging wearable technology, electronic devices with integrated thermal management capabilities are highly desired [3]. Therefore, it is essential to develop high-performance electromagnetic shielding and thermal management materials to meet the requirement of various wearable electronic devices, as well as to protect humans from electromagnetic radiation.

Due to the shortcomings of heavy weight, high cost and poor flexibility, traditional electromagnetic shielding materials based on metals can no longer meet the requirements of modern electronic devices for light-weight and flexible EMI shielding [4]. As an alternative to metals, conductive polymer composites have been explored extensively in the past few years due to their lightweight, high flexibility, together with effective and tunable EMI shielding effectiveness and joule heating performance [5-7]. Many conductive components, such as silver nanoparticles (AgNPs)/nanowires (AgNWs) [8-10], carbon nanotubes (CNTs) [11, 12], graphene [13] and new emerging transition metal carbide/carbonitride (MXene) [14, 15] and their hybrids [16], have been employed as fillers or coating materials to construct conductive polymer composites. Among these, AgNWs have excellent transparency, conductivity, flexibility and hence have been used extensively in fabricating conductive polymer composites with high EMI shielding and electrical heating performances [17-20]. One of the most commonly used method to combine AgNWs with polymers is to coat AgNWs on the surface of various polymer substrates [8, 17, 21, 22]. However, several problems associated with AgNWs, including easy oxidation, large wire-to-wire junction resistance and poor adhesion to polymer substrates, need to be addressed considering the long-term practical applications of their polymer composites [23]. In order to solve those problems, an over-coating layer was generally introduced to protect the AgNWs [24] and at the same time improve the adhesion to the substrates [25].

However, the incorporation of nonconductive protecting layer will inevitably decrease the electrical conductivity and thus lead to diminished EMI shielding and electrical heating performance of the resultant materials. Consequently, conductive polymer coating such as polyaniline or polypyrrole has been introduced [26, 27]. However, the drawbacks of poor solubility in different solvents, difficulty in processing and irreproducibility have reduced their applicability. Among various conductive polymers, poly(3,4-ethylenedioxythiophene):poly(styrenesulfonate) (PEDOT:PSS) has been demonstrated as a promising candidate for producing conductive coatings, not only owing to its superior inherent characteristics including high electrical conductivity, excellent dispersibility in various solvents and high transparency [28], but also the advantage of easy fabrication through a simple and highly reproducible process [29].

Due to the advantages of light-weight and porous structure, nonwoven fabrics have been exploited as an ideal substrate for constructing various composites with desirable EMI shielding and electrical heating performances [30-32]. Herein, we demonstrate a facile dip-coating approach for fabricating flexible and highly conductive AgNWs decorated poly-m-phenyleneisophthalamide (PMIA) nonwoven fabric. **PEDOT:PSS was employed as an over-coating layer to improve the adhesion of AgNWs and PMIA fibers and the thermal stability of AgNWs. The electrical conductivity and EMI shielding effectiveness of the PMIA/AgNWs nonwoven fabric were enhanced after PEDOT:PSS coating.** The Joule heating performance of the functionalized PMIA nonwoven fabric was also investigated.

2. Experimental

2.1. Materials

PMIA nonwoven fabric with thickness of 0.3 mm was provided by Jiangsu Kaidun New Material Co., Ltd, China. AgNWs (ethanol dispersion with 1g AgNWs per 100 ml

ethanol) were purchased from Beijing Deke Daojin Science and Technology Co., Ltd, China. Poly (3,4-ethylene dioxythiophene/polystyrene sulfonate) (PEDOT: PSS) was purchased from Shanghai Ouyi Organic Photoelectric Materials, China. Ethanol dimethyl sulfoxide (DMSO) were purchased from Sinopharm Chemical Reagent Co., Ltd, China.

2.2. Preparation of PMIA/AgNWs/PEDOT Composites

Firstly, the aramid non-woven fabric was washed with deionized water to remove the impurities on the surface and dried at 50 °C in a vacuum oven. Secondly, the cleaned aramid nonwovens were immersed in ethanol dispersion of AgNWs with different concentrations of 0.1 wt%, 0.2 wt%, 0.3 wt% and 0.4 wt% for different periods of time. The AgNWs ethanol dispersions with 0.1-0.4 wt.% concentration were prepared by diluting a commercial AgNW dispersion with certain amount of ethanol. After being dried in vacuum oven at 50 °C, the PMIA /AgNWs nonwoven fabric was immersed in aqueous solution of PEDOT: PSS (prepared by mixing of 18 g PEDOT:PSS and 1 g DMSO) for 1 min, and then dried at room temperature for 30 min followed by being dried 50 °C under vacuum for 12 h. The obtained sample was denoted as PMIA/AgNWs/PEDOT:PSS. The procedure for preparing PMIA/AgNWs/PEDOT:PSS nonwoven fabric is shown schematically in Figure 1.

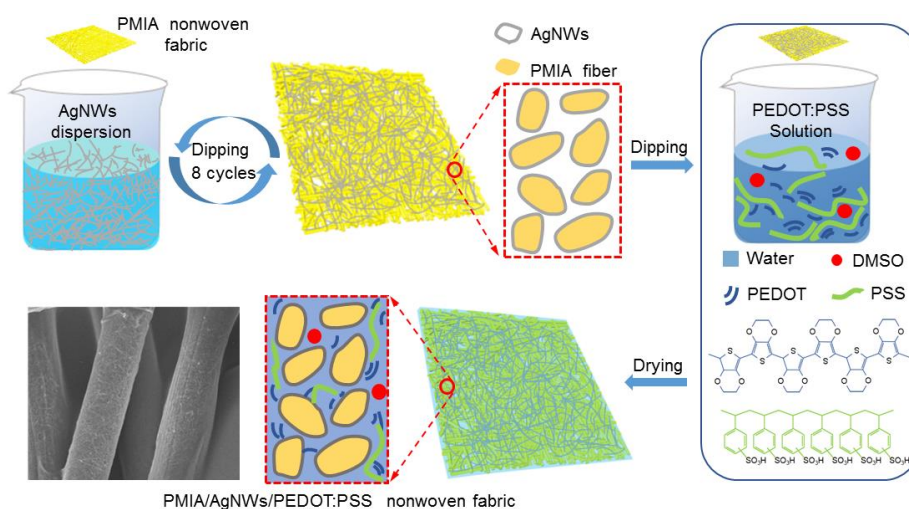


Figure 1. Schematic illustration of the procedure for preparing

PMIA/AgNWs/PEDOT:PSS nonwoven fabric

2.3. Characterization and Measurement

The surface morphology of nonwoven fabric was observed by using a field emission scanning electron microscope (FE-SEM, Regulus 8100, Hitachi, Japan). The chemical composition was analyzed by exploiting an X-ray photoelectron spectroscopy (XPS, ESCALAB 250XI, Thermo Fisher Scientific, USA) with an Al K α X-ray source (1486.6 eV photons). The crystalline structural features of pristine PMIA and PMIA/AgNWs nonwoven fabrics were identified by using an X-ray diffractometer (XRD, Rigaku Ultima IV, Japan). The thermal property of pristine PMIA and PMIA/AgNWs and PMIA/AgNWs/PEDOT:PSS nonwoven fabrics was studied by using a TG/DSC thermal analyzer (STA 449 F3, NETZSCH GmbH, Germany). The measurement was conducted in nitrogen atmosphere from 40 to 800 °C with a heating rate of 20 °C/min. The mechanical properties were measured by using a universal tensile testing machine (Instron 5965, USA). Rectangular specimens (20 mm \times 10 mm) were used for tensile tests. The electrical sheet resistance was measured by using a four probe resistance measuring instrument (ST-2258C, Suzhou Jingge Electronic Co., Ltd, China). The electrical properties upon bending were investigated by employing a precision power supply (B2901A, Keysight, USA). For Joule heating performance test, the nonwoven fabric with a dimension of 50 mm \times 20 mm was used with the working distance of 20 mm. Conductive copper tape as the electrode was mounted on both ends of the nonwoven fabric. Voltages were applied to by using the precision power supply (B2901A, Keysight, USA). The surface temperature was measured by using a contact thermometer (UT320A, Uni-Trend Technology Co. Ltd, China). The infrared thermal images were captured by using an infrared thermal imager (TiS50, Fluke Electronic Instrumentation, USA). The EMI shielding performance was measured by using an

ENA network analyzer (ZNB 20, Rohde & Schwarz, Germany) by means of waveguide method. The scattering parameters were recorded in the frequency range of 8.2-12.4 GHz and used to calculate the coefficients. The total EMI SE (SE_T), reflection loss (SE_R), absorption loss (SE_A), multiple internal reflections (SE_M) and power coefficients of transmission (T), reflection (R) and absorption (A) were calculated based on the S parameters as follows:

$$R = |S_{11}|^2 = |S_{22}|^2 \quad (1)$$

$$T = |S_{21}|^2 = |S_{12}|^2 \quad (2)$$

$$A = 1 - R - T \quad (3)$$

$$SE_R = -10 \log(1 - R) \quad (4)$$

$$SE_A = -10 \log\left(\frac{T}{1-R}\right) \quad (5)$$

$$SE_T = SE_A + SE_R + SE_M \quad (6)$$

where SE_M can be ignored in cases when the absorption loss is higher than 10 dB [33].

3. Results and discussion

3.1 Morphology, XRD, XPS and electrical conductivity of PMIA/AgNWs/PEDOT:PSS nonwoven fabric

Figure 2a shows the surface appearance of PMIA nonwoven fabric before and after being dipped with AgNWs ethanol dispersion. It can be seen that after the ethanol evaporated, the color of the PMIA nonwoven fabric changed from white (the upper image in Figure 2a) to grey (the lower image in Figure 2a). Compared with the morphology of pristine PMIA nonwoven fabric (Figure 2b and c), the individual fibers in PMIA/AgNWs nonwoven fabric were uniformly coated with a percolated network of randomly oriented AgNWs (Figure 2e and f). The effect of AgNWs dispersion concentration and dipping times on the electrical conductivity of the PMIA/AgNWs nonwoven fabric was investigated. As can be seen from Figure 2d, for the same AgNWs

dispersion concentration, the electrical sheet resistance of all PMIA/AgNWs nonwoven fabric samples decreased obviously (maximum 85.82% and minimum 70.60%) as the number of dip-coating cycles increased from 1 to 8 times, indicating enhanced electrical conductivity. When the dipping cycle increased from 8 to 10 times, the sheet resistance only changed slightly, showing that 8 cycles of dipping was sufficient. For the same dipping cycle, the sheet resistance also decreased with increasing AgNWs dispersion concentration. In particular, when the AgNWs dispersion concentration was 0.3 wt%, a sheet resistance of $0.97 \pm 0.07 \text{ } \Omega/\text{sq}$ was achieved after 8 dipping cycles, which was relatively close to the sheet resistance of the PMIA/AgNWs nonwoven fabric dipped into the 0.4 wt% dispersion for 8 times ($0.80 \pm 0.08 \text{ } \Omega/\text{sq}$). Therefore, PMIA nonwoven fabric sample immersed in 0.3 wt% AgNWs dispersion solution for 8 times was chosen for following PEDOT:PSS coating.

XPS was used to confirm the successful deposition of AgNWs on the PMIA nonwoven fabric. Figure 2h shows the XPS wide scan of pristine and PMIA/AgNWs nonwoven fabrics. Compared with the spectrum of PMIA nonwoven fabric, the spectrum of PMIA/AgNWs nonwoven fabric showed strong signal of Ag at a BE of about 370 eV, indicating the presence of silver in the PMIA/AgNWs nonwoven fabric [34]. The core-level spectrum of Ag 3d (Figure 2h) consisted of two peak components of Ag 3d_{3/2} at BEs of 374.0 eV and Ag 3d_{5/2} at 368.0 eV, respectively. Those peaks were attributed to the Ag⁰ species, confirming that the deposited AgNWs in the PMIA nonwoven fabric was in zerovalent state.

XRD was performed to further confirm the deposition of AgNWs. As shown in Figure 2i, compared with the XRD pattern of pristine PMIA nonwoven fabric, the PMIA/AgNWs nonwoven fabric showed five distinct characteristic peaks at 2θ values of 38.2° , 44.4° , 64.6° , 77.4° , and 81.6° , which correspond to the (1 1 1), (2 0 0), (2 2

0), (3 1 1), and (2 2 2) fcc crystal planes of AgNWs, demonstrating that AgNWs successfully deposited on the PMIA fiber surface. No diffraction peak for silver halide or silver oxide was observed in the XRD pattern of PMIA/AgNWs nonwoven fabric, suggesting that the AgNWs covered on the surface of PMIA fibers were in elemental form.

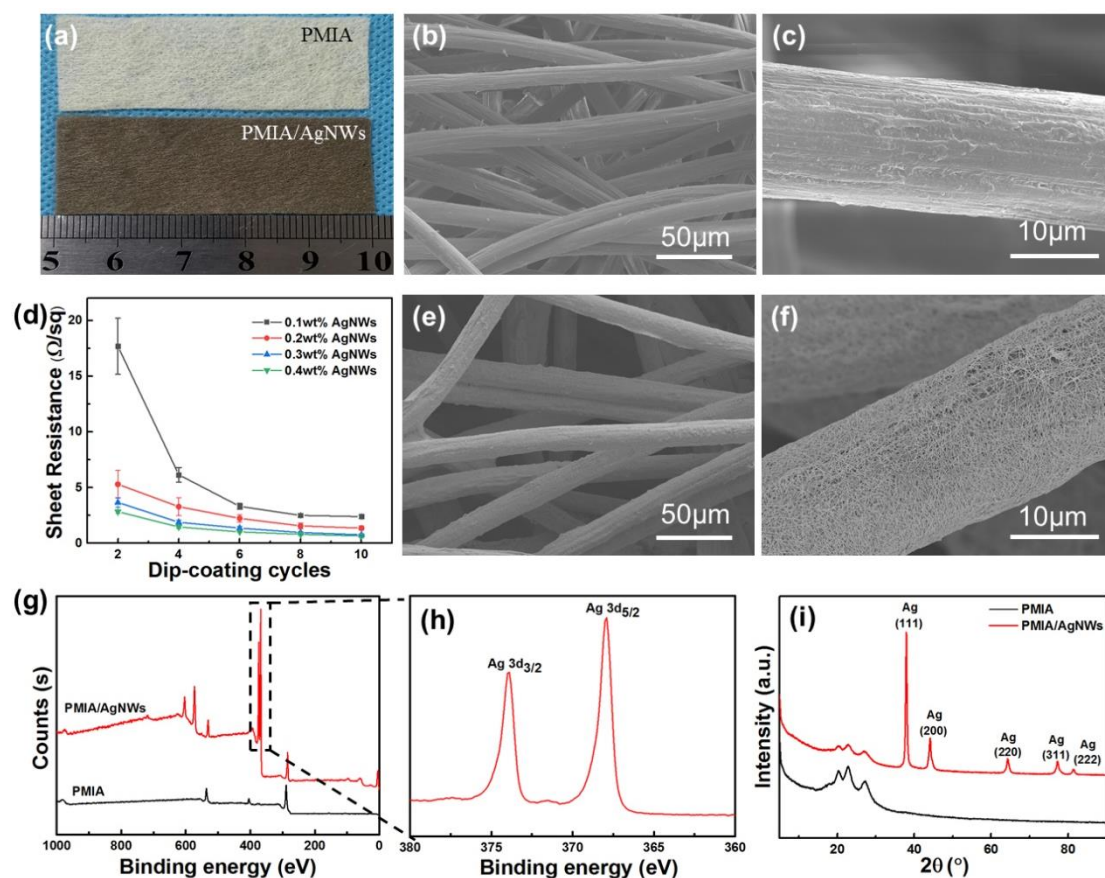


Figure 2. Digital image of PMIA (upper) and PMIA/AgNWs (lower) nonwoven fabric (a); SEM images of PMIA nonwoven fabric (b and c); the change of electrical sheet resistance of PMIA/AgNWs nonwoven fabric with AgNWs dispersion concentration and dipping times (d); SEM image of PMIA/AgNWs nonwoven fabric (e and f); XPS wide scan (g) and Ag3d spectrum (h) of PMIA/AgNWs nonwoven fabric; XRD pattern of PMIA and PMIA/AgNWs nonwoven fabric (i).

PMIA/AgNWs/PEDOT:PSS nonwoven fabrics were prepared by immersing PMIA/AgNWs samples into the PEDOT:PSS aqueous solution. After the evaporation

of water, the PMIA/AgNWs were uniformly wrapped with a layer of PEDOT:PSS to form the desired PMIA/AgNWs/PEDOT:PSS nonwoven fabric with good flexibility (as shown in Figure 3a). SEM images in Figure 3b and c revealed that the deposited AgNWs were tightly embedded in PEDOT:PSS matrix. This matrix acted as the adhesion layer between the AgNW networks and PMIA fibers due to the capillary force during the solvent evaporation process of aqueous solution of PEDOT:PSS [35]. In addition, PEDOT:PSS bridged the void spaces between adjacent AgNWs and provided additional conducting paths. Figure 3d and e show the XPS wide scan and S2p core-level spectrum of PMIA/AgNWs/PEDOT:PSS nonwoven fabric, respectively. The S2p core-level spectrum showed the BEs at 164.2 eV for the sulfur signal of PEDOT and 168 eV for the sulfur signal of PSS [28], indicating the successful coating of PEDOT:PSS layer. After coating the PEDOT:PSS on the PMIA/AgNWs, the sheet resistance decreased by 5.15% to $0.92 \pm 0.06 \Omega/\text{sq}$. As shown in Figure 3f, the connected light-emitting diode (LED) bulbs forming the logo of “QDU” was lighted with a power supply of 36 V when the PMIA/AgNWs/PEDOT:PSS nonwoven fabric was connected in the circuit.

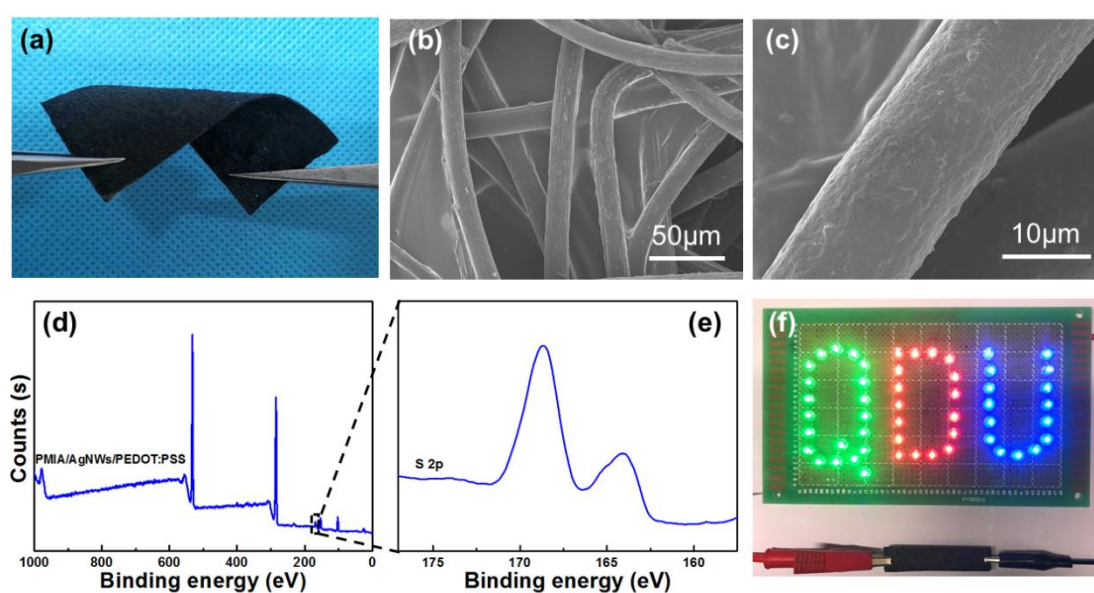


Figure 3. Digital image showing high flexibility (a), SEM images at different

magnifications (b) and (c), XPS wide scan (d) and S2p spectra (e), the logo of “QDU” lighted with a power supply of 36 V when the PMIA/AgNWs/PEDOT:PSS nonwoven fabric was connected in the circuit (f).

3.2 Effect of PEDOT:PSS coating on the bonding fastness and thermal stability of AgNWs

To evaluate the effect of PEDOT:PSS on improving the adhesion between AgNWs and PMIA nonwoven fabric substrate, a peel-off test was conducted manually by using a commercial tape. The electrical sheet resistance of PMIA/AgNWs and PMIA/AgNWs/PEDOT:PSS nonwoven fabrics after peel-off test was measured to quantify the improved adhesion after PEDOT:PSS coating. As can be seen from Figure 4a, the sheet resistance of PMIA/AgNWs nonwoven fabric increased substantially from $0.97 \pm 0.07 \text{ } \Omega/\text{sq}$ to $80.48 \pm 3.13 \text{ } \Omega/\text{sq}$ after 3 times of peel-off. The sheet resistance was too high to be measured after being peeled off for 4 times, indicating the loss of electrical conductivity. SEM images in Figure 4b and c show that the AgNWs on the PMIA fibers were peeled off after 3 peeling off tests. In contrast, the sheet resistance of PMIA/AgNWs/PEDOT:PSS nonwoven fabric only increased from $0.92 \pm 0.06 \text{ } \Omega/\text{sq}$ to $1.51 \pm 0.14 \text{ } \Omega/\text{sq}$ after 3 peel-off tests. As can be seen from Figure 4d and e, the surface of PEDOT:PSS coating maintained well after the same peeling off tests. The above results suggest that the adhesion between AgNWs and PMIA nonwoven fabric was greatly improved after PEDOT:PSS coating. This could be attributed to the strong physical adsorption and van der Waals force of the PEDOT chains on PMIA nonwoven fabric which had high porosity and large surface area [36].

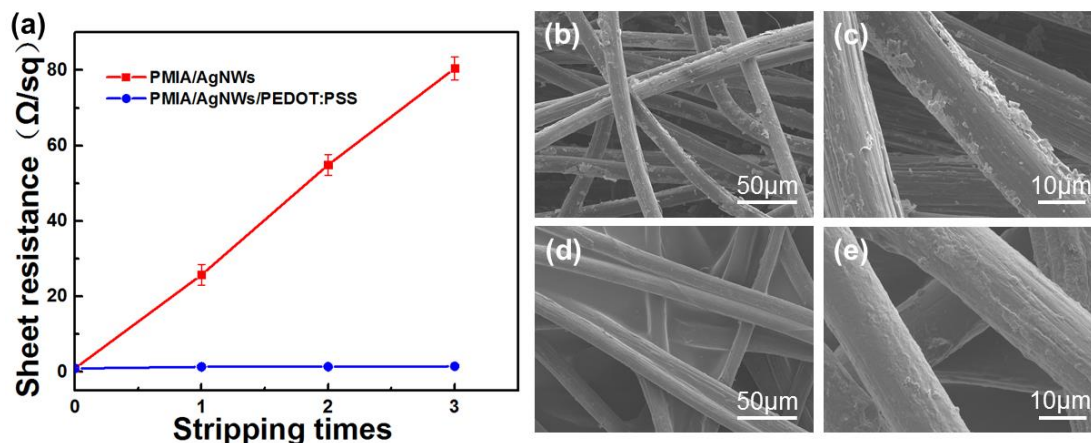


Figure 4. The change of sheet resistance with stripping times for PMIA/AgNWs and PMIA/AgNWs/PEDOT:PSS nonwoven fabric (a); SEM image of PMIA/AgNWs (b, c) and PMIA/AgNWs/PEDOT:PSS (d, e) nonwoven fabric after 3 peel-off tests.

Thermal stability of the conductive nonwoven fabrics is very important for their application as electrical heaters. Previous study showed that AgNWs would decompose into nanoparticles at temperatures above 200 °C [37]. The sheet resistance of PMIA/AgNWs and PMIA/AgNWs/PEDOT:PSS nonwoven fabric after being heated at different temperatures was measured and plotted against the initial sheet resistance. It can be seen in Figure 5a that the sheet resistance of PMIA/AgNWs nonwoven fabric increased by 12.6% and 24.8% after being treated at 50 °C and 100 °C for 1 h respectively. The R/R_0 increased to 2.10 after being treated at 150 °C for 1 h and further increased significantly to 84.37 after being treated at 200 °C for 1 h. After being treated at 250 °C for 1 h, the sheet resistance of PMIA/AgNWs nonwoven fabric could not be measured, indicating the loss of electrical conductivity. Figure 5b and c shows SEM images of PMIA/AgNWs nonwoven fabric after heating at 200 °C for 1 h. The decomposition of the AgNWs into nanoparticles can be clearly seen on the PMIA fibers. The fusing of AgNWs decreased their junctions and consequently led to the decrease in electrical conductivity. In contrast, the R/R_0 of PMIA/AgNWs/PEDOT:PSS nonwoven fabric maintained nearly unchanged after being treated at the temperature of 150 °C and

only increased slightly to 1.94 after being treated at 200 °C for 1 h. The SEM image in Figure 5d shows PEDOT:PSS coating layer remained on the nonwoven fabric after heating at 200 °C for 1 h. These results suggest thermal stability of the PMIA/AgNWs/PEDOT:PSS nonwoven fabric was greatly improved compared with that of PMIA/AgNWs nonwoven fabric.

Mechanical properties are crucial for the practical applications of conductive polymer composites. Figure 5e shows the stress-strain curves of PMIA, PMIA/AgNWs and PMIA/AgNWs/PEDOT:PSS nonwoven fabrics while the average tensile strength and elongation at break are given in Figure 5f. As the PMIA nonwoven fabric is randomly oriented fiber network, the low physical entanglement among the fibers allow them easily to be pulled apart, resulting in a lower tensile strength and a greater elongation at break. The deposition of AgNWs strengthened the fiber network, which increased the tensile strength and lowered the elongation at break slightly. The introduction of PEDOT:PSS coating layer filled in the void gaps among the individual fibers and therefore increased the tensile strength to 11.7 ± 0.42 MPa, but the elongation at break decreased to $24.89\% \pm 2.45$ as the deformation of fibers was restricted.

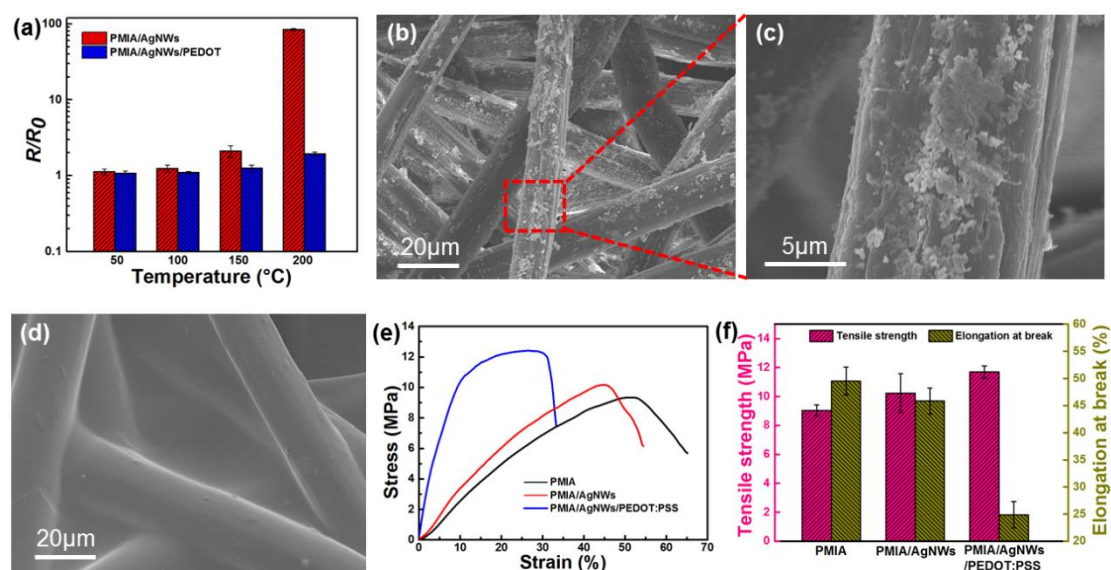


Figure 5. The electrical resistance of PMIA/AgNWs and PMIA/AgNWs/PEDOT:PSS

nonwoven fabrics after being treated at different temperature for 1 h (a); the SEM image of PMIA/AgNWs (b, c) and PMIA/AgNWs/PEDOT:PSS (d) being treated at 200°C for 1 h; the stress-strain curves (e), the tensile strength and elongation at break (f) of PMIA, PMIA/AgNWs and PMIA/AgNWs/PEDOT:PSS nonwoven fabrics.

3.4 EMI shielding performance of PMIA/AgNWs/PEDOT:PSS nonwoven fabric

The feasibility of using the developed highly conductive and flexible PMIA/AgNWs/PEDOT:PSS composite nonwoven fabric in the field of high-performance EMI shielding was investigated here. Figure 6a shows the EMI shielding effectiveness of PMIA, PMIA/AgNWs and PMIA/AgNWs/PEDOT:PSS nonwoven fabrics. It can be seen that the EMI SE of pristine PMIA nonwoven was close to zero, indicating no EMI shielding ability; after deposition of AgNWs, the EMI SE of PMIA/AgNWs reached an average value of 52.6 dB and in particular, after being coated by conductive PEDOT:PSS, the average EMI SE of PMIA/AgNWs/PEDOT:PSS nonwoven fabric increased to 56.6 dB. According to Simon formalism [38], the EMI SE of electrically conductive materials are positively correlated with their electrical conductivity and thickness. Compared with PMIA/AgNWs nonwoven fabric, PMIA/AgNWs/PEDOT:PSS nonwoven fabric achieved both increased electrical conductivity and thickness (the thickness of PMIA/AgNWs and PMIA/AgNWs/PEDOT:PSS nonwoven fabric was 0.310 mm and 0.446 mm respectively), therefore exhibiting a higher EMI SE.

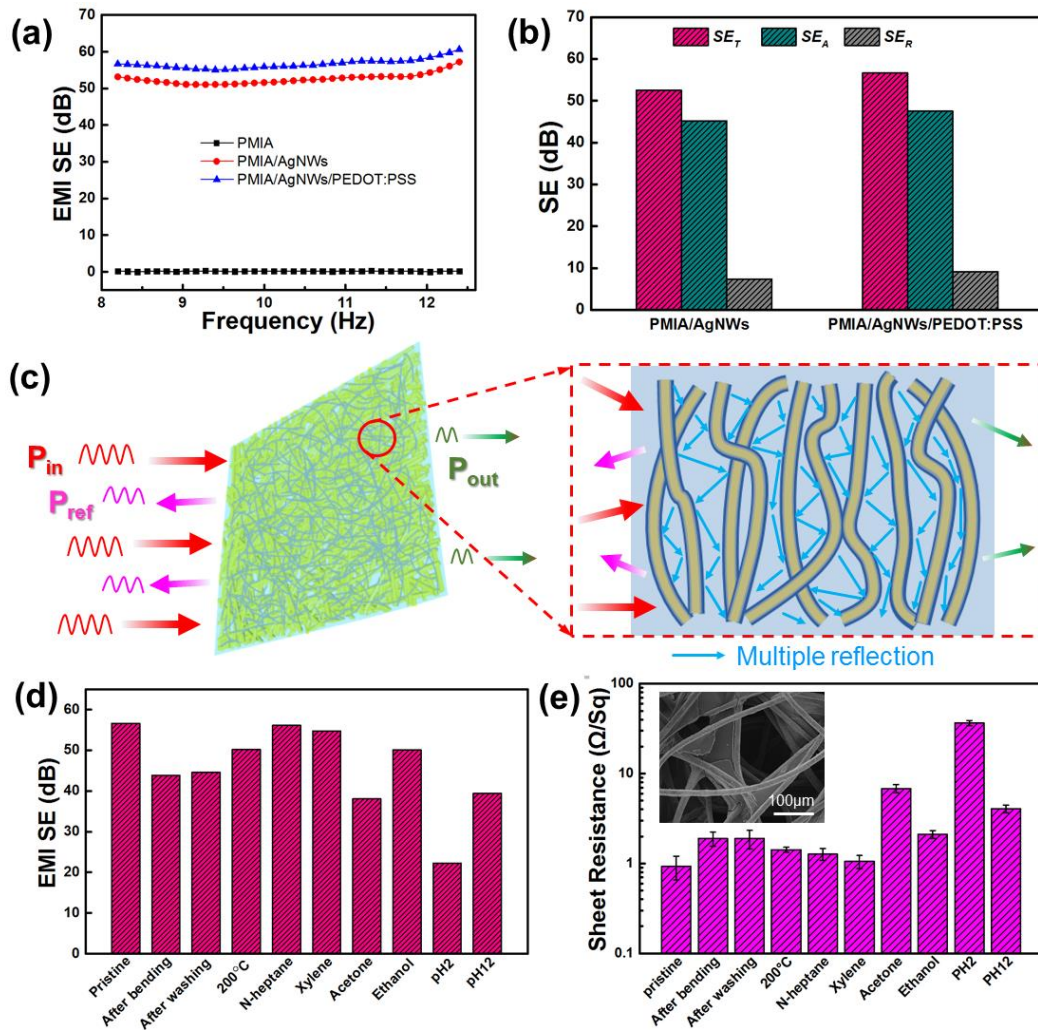


Figure 6. The EMI SE over 8.2-12.4 GHz of PMIA, PMIA/AgNWs and PMIA/AgNWs/PEDOT:PSS nonwoven fabrics (a); the average SE_T , SE_A and SE_R of PMIA/AgNWs/PEDOT:PSS (b); the transmission process of EM waves (c); the EMI SE (d) and sheet resistance (e) of pristine PMIA/AgNWs/PEDOT:PSS, PMIA/AgNWs/PEDOT:PSS after ultrasonic washing for 2h, 1000 bending cycles, being treated at 200 °C for 1h and immersed in acid/alkali solution and various organic solvents for 3 days, the inserted image in (e) shows SEM image of PMIA/AgNWs/PEDOT:PSS nonwoven fabric treated with acid solution for 2h. To elucidate the EMI shielding mechanism, the total EMI shielding effectiveness (SE_T), the effectiveness of reflection loss (SE_R) and absorption loss (SE_A) were calculated by using Eqn. 4 and 5. As can be seen from Figure 6b, the average SE_A was much higher

than SE_R for both PMIA/AgNWs and PMIA/AgNWs/PEDOT:PSS nonwoven fabrics. However, this is not sufficient to conclude that the shielding mechanism is absorption dominant because EMI shielding often involves both reflection and absorption loss. As shown in Figure 6c, when the incident EM waves propagated to the surface of PMIA/AgNWs/PEDOT:PSS nonwoven fabric, part of them were reflected due to the impedance mismatch at the interface between air and PMIA/AgNWs/PEDOT:PSS nonwoven fabric, causing reflection loss. The other part entering the PMIA/AgNWs/PEDOT:PSS nonwoven fabric were reflected multiple times across large amounts of surface area of fibers in the porous nonwoven fabric, the energy attenuated, causing absorption loss [39]. As reflection occurred before absorption, the SE_A value only represents the ability to absorb EM waves penetrating into the materials excluding the reflected waves [40, 41]. The power coefficients of R and A , representing the actual reflection and absorption of the EM waves, are often used to study the shielding mechanism [31, 33, 42, 43]. The power coefficients of R and A for PMIA/AgNWs/PEDOT:PSS nonwoven fabric were 0.85 and 0.15 respectively, indicating that most of the EM waves were reflected by the PMIA/AgNWs/PEDOT:PSS nonwoven fabric with high electrical conductivity.

Skin depth (δ), denoted as the depth where the intensity of EM waves drops to $1/e$ of its original value, is an important parameter in reflecting the shielding ability and can be calculated by $\delta = (\pi f \mu \sigma)^{-1/2}$, when $\sigma \gg 2\pi f \epsilon_0$, where f is the frequency, σ is the electrical conductivity, μ is the magnetic permeability ($\mu = \mu_0 \mu_r$, $\mu_0 = 4\pi \times 10^{-7} \text{ Hm}^{-1}$ and $\mu_r = 1$ for nonmagnetic materials) and ϵ_0 represents the vacuum permittivity. The calculated δ values for PMIA/AgNWs/PEDOT:PSS nonwoven fabric were 0.113 mm and 0.092 mm at 8.2 GHz and 12.4 GHz respectively, which was lower than its thickness (0.446 mm) and thus contributed to the a high EMI SE [30, 44].

The theoretical EMI SE of the PMIA/AgNWs/PEDOT:PSS nonwoven fabric was calculated by exploiting the following equations:

$$SE_A = 8.7d\sqrt{\pi f\mu\sigma} = 8.7\frac{d}{\delta} \quad (7)$$

$$SE_R = 39.5 + 10\log\frac{\sigma}{2\pi f\mu} \quad (8)$$

Where d is the sample thickness, f , σ , μ and δ are defined as above.

The calculated value of SE_A and SE_R at 12.4 GHz was 42.26 dB and 23.47 dB, respectively, contributing to an SE_T of 65.73 dB; the calculated value of SE_T at 8.2 GHz was 59.63 dB (SE_A of 34.37 dB and SE_R of 25.26 dB). Those theoretical results of SE_T were in good agreement with the experimental value (61.37 dB at 12.4 GHz and 56.82 dB at 8.2 GHz). The theoretical value of R was 0.995, which was higher than its experimental value (0.85), while the theoretical result of A was 0.005, which was lower than its experimental value (0.15). The higher experimental value of A can be explained by the fact that PMIA/AgNWs/PEDOT:PSS nonwoven fabric had a porous structure with high fiber surface area, in which the EM waves were reflected and scattered for multiple times, and were finally absorbed or dissipated as heat [2].

EMI shielding performance under mechanical deformation and chemical environment is highly desirable for practical applications. Therefore, the EMI shielding performance of PMIA/AgNWs/PEDOT:PSS nonwoven fabric after bending, washing, high-temperature treatment and various chemical corrosion was evaluated. As can be seen from Figure 6d, the average EMI SE over X-band of PMIA/AgNWs/PEDOT:PSS nonwoven fabric changed from 56.6 dB to 43.87, 44.57 and 50.19 after 1000 bending times, washing under ultrasonication for 2h and treated at 200 °C for 1 h, respectively; different changes in EMI SE values of PMIA/AgNWs/PEDOT:PSS nonwoven fabric were observed after being treated with various organic solvents including n-heptane, xylene, acetone and ethanol, as well as acid and base solutions. In particular, the sample

treated with acid solution with $\text{pH} = 2$ showed the lowest EMI SE of 22.29 dB, which still meet the industrial requirement of 20 dB [45]. The obvious decrease in EMI SE after acid soaking is because the H^+ in the acid solution combined with the PSS^- , resulting the phase separation of PEDOT:PSS and subsequently the removal of part PSS protecting layer [46] (as shown in the inserted SEM image in Figure 6e). In addition, the infiltration of the acid solution also caused the oxidization of AgNWs [40], and hence decreased the electrical conductivity of the PMIA/AgNWs/PEDOT:PSS nonwoven fabric (Figure 6e) and led to diminished EMI SE.

3.4 Joule heating performance of the PMIA/AgNWs/PEDOT:PSS nonwoven fabric

In addition to the high EMI shielding effectiveness and reliable mechanical properties, the Joule heating performances of PMIA/AgNWs/PEDOT:PSS nonwoven fabric was also investigated for use as electrical heaters. Figure 7a shows the relationship between surface temperature and voltage for a PMIA/AgNWs/PEDOT:PSS nonwoven fabric based electrical heater. It can be seen that the heater reached the highest temperature of 152 °C at an applied voltage of 2.9 V and then sharply dropped to 43.8 °C with further increasing voltages. Figure 7b shows the change of T_s with the four-step change in voltage first from 0.3 V to 2.0 V and then to 0.3 V. When the voltage was changed by 0.5 V, the surface temperature of PMIA/AgNWs/PEDOT:PSS electrical heater was found to change by 36%-78%, showing rapid and striking response. This indicates that the PMIA/AgNWs/PEDOT:PSS nonwoven fabric has great potential to be used as an electrical heating devices with good temperature management. Figure 7c shows the change of saturation temperature (T_s) under different applied voltages. It can be seen that T_s increased as increasing voltage because of the more generated Joule heat power. It can also be noted that the PMIA/AgNWs/PEDOT:PSS nonwoven fabric could be heated from room temperature to T_s within 20 s, indicating rapid heating response to

voltage; when the power was switched off, the surface temperature decreased to room temperature within 30 s, indicating the rapid cooling response. At a low voltage of 2 V, the PMIA/AgNWs/PEDOT:PSS electrical heater reached a T_s of around 110 °C, which was higher than previous values reported electrical heaters based on AgNWs based polymer composites [17, 20].

The PMIA/AgNWs/PEDOT:PSS based electrical heater also showed high long-time stability as demonstrated by the stable T_s at around 55 °C for a period of 10000 s under a constant voltage of 1 V (Figure 7d). Figure 7e shows the change in surface temperature upon an alternating voltage of 0 V and 1 V. It can be seen that the PMIA/AgNWs/PEDOT:PSS electrical heater showed highly repeatable alterations in surface temperature between about 25 °C and 55 °C for 10000 s (200 cycles).

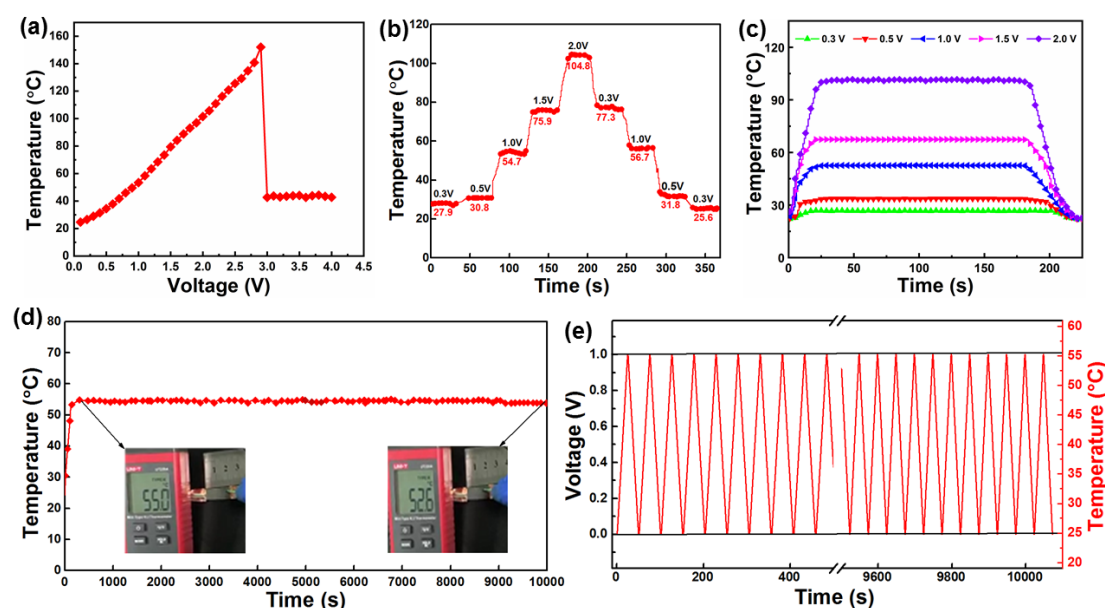


Figure 7. The relationship between surface temperature and voltage (a); surface temperature upon gradually changed voltages (b); time-dependent temperature at different supplied voltage (c); the long-term stability upon a supplied voltage of 1.0 V (d) and the heating repeatability upon alternating voltage of 0 V/1 V (e) for PMIA/AgNWs/PEDOT:PSS electrical heater.

The electrical heating performance and sheet resistance were measured under different

bending conditions to assess the reliability of the PMIA/AgNWs/PEDOT:PSS nonwoven fabric as flexible electrical heaters. As shown in Figure 8a, a PMIA/AgNWs/PEDOT:PSS sample with dimensions of 40 mm × 10 mm was subjected to outward bending under a constant voltage of 1.0 V. The surface temperature showed an increase from 46.3 °C to 55.1 °C with the decreasing chord length from 40 mm to 20 mm (Figure 8a). This is because during the bending process, the adjacent individual fibers tended to contact each other to form tight conductive networks, which enhanced the electrical conductivity of the nonwoven fabric [47]. The stable electrical-mechanical property and joule heating performance of PMIA/AgNWs/PEDOT:PSS nonwoven fabric were evaluated through repeated bending-relaxation cycles at a bending chord length of 20 mm. As shown in Figure 8b, the electrical resistance increased slightly by 5.2% from 2.88 Ω to 3.03 Ω after 1000 bending/releasing cycles. This could be attributed to the enhanced AgNWs-AgNWs and AgNWs-PMIA fibers adhesion, which prevented the sliding of conductive layer at the interface during bending. As a distinct contrast, the R/R_0 of PMIA/AgNWs nonwoven fabric without PEDOT:PSS coating increased remarkably by 86% from 5.54 Ω to 10.30 Ω after 1000 bending/releasing cycles (Figure 8c) due to the slipping and/or delamination of AgNWs [48]. These results also confirmed the improved adhesion between AgNWs and PMIA nonwoven fabric after PEDOT:PSS coating. The excellent electrical conductivity stability upon bending could endow the PMIA/AgNWs/PEDOT:PSS nonwoven fabric with stable heating performance during practical applications.

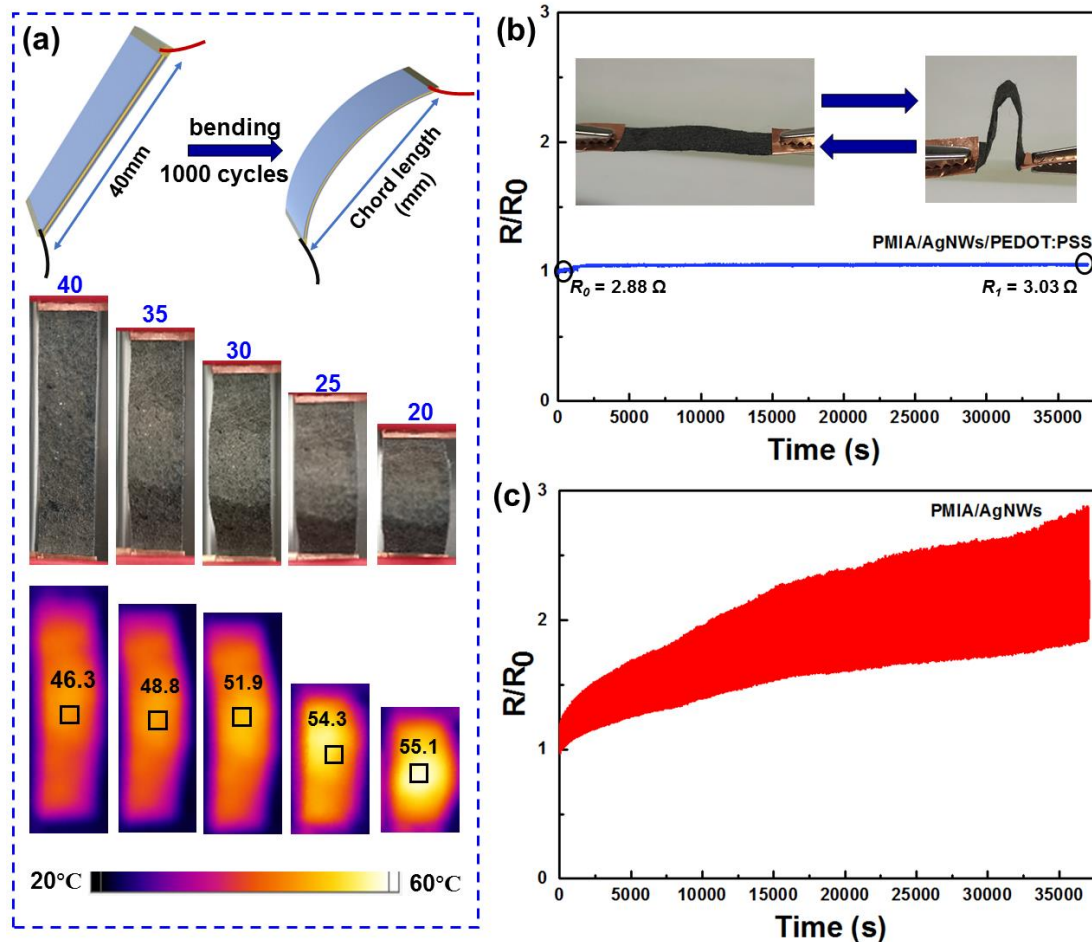


Figure 8. Illustration of the bending test, the digital images and IR image of PMIA/AgNWs/PEDOT:PSS under different bending conditions (a); real-time relative change of electrical resistance for PMIA/AgNWs/PEDOT:PSS (b) and PMIA/AgNWs (c) upon repeated bending and releasing.

We here demonstrated the feasibility of using PMIA/AgNWs/PEDOT:PSS nonwoven fabric as electrical heaters for personal thermal management. Informed consent was obtained from the human volunteer before conducting the experimental study. Figure 9 shows the IR images of the electrical heaters attached to human index finger, wrist and ankle with supplied voltages of 0, 0.5 and 1.0 V, respectively. With a low supplied voltage of 0.5 V, the electrical heaters affixed to the figure, wrist and knee were heated from room temperature of about 26.5 °C to about 33.6 °C, which is in the range of comfortable temperature (between 33 and 38 °C) for human body [49]. When the

supplied voltage increased to 1.0 V, the heater temperature reached around 52.7 °C, which could be used to relieve joint pain and stiffness [50].

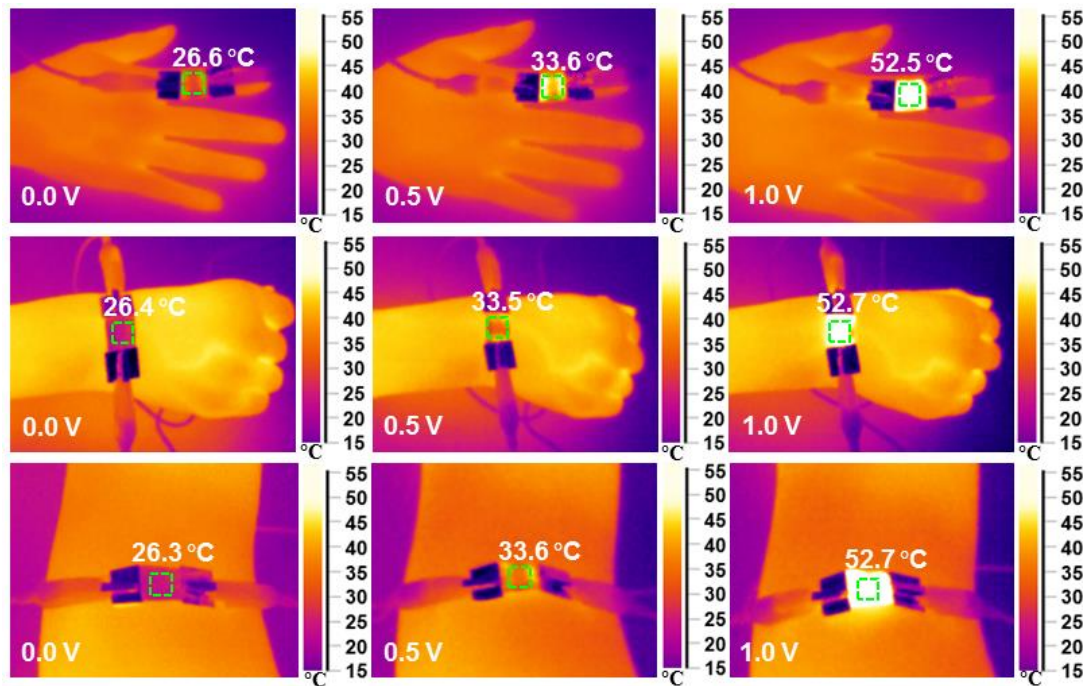


Figure 9. The IR images of electrical heaters based on PMIA/AgNWs/PEDOT:PSS nonwoven fabric attached to human finger (a), wrist (b) and ankle (c) with supplied voltages of 0 V, 0.5 V and 1.0 V.

4. Conclusions

Flexible and electrically conductive PMIA nonwoven fabric consisting of AgNWs/PEDOT:PSS composite coated on a commercial PMIA nonwoven fabric was prepared through a two-step dipping coating method. The fabricated flexible PMIA/AgNWs/PEDOT:PSS composite nonwoven fabric exhibited an electrical resistance as low as $0.92 \pm 0.06 \Omega/\text{sq}$. The PEDOT:PSS as the over-coating layer improved the adhesion between AgNWs and PMIA nonwoven fabric and protected the AgNWs from decomposition at high temperature. The high electrical conductivity of the PMIA/AgNWs/PEDOT:PSS nonwoven fabric endowed it with excellent EMI shielding and Joule heating performances. For a single layer of

PMIA/AgNWs/PEDOT:PSS nonwoven fabric, the EMI SE reached 56.6 dB over X-band and was above the industrial requirement after being washed, bended and treated with acid/alkali solution and various organic solvents. The electrical heaters based on PMIA/AgNWs/PEDOT:PSS nonwoven fabric could reach a saturation temperature of around 110 °C at a low voltage of 2 V and exhibited rapid response to the voltage on/off switching. The heaters also presented reliable heating stability and repeatability during long-term and repeated heating/cooling cycles. Owing to its simple and low cost fabrication procedures, reliable stability under high temperature and mechanical deformations, enhanced EMI shielding and Joule heating performances, the PMIA/AgNWs/PEDOT:PSS nonwoven fabric holds great promise for use in wearable protective devices and high-performance heating components.

Acknowledgements

The authors would like to thank the financial support from the Shandong Provincial Natural Science Foundation (Grant no. ZR2020QE087), the Shandong Provincial Key Research and Development Program (Grant no. 2019GGX102071) and the Shandong “Taishan Youth Scholar Program” (Grant no. tsqn201909100).

References

- [1] X. Yang, S. Fan, Y. Li, Y. Guo, Y. Li, K. Ruan, S. Zhang, J. Zhang, J. Kong, J. Gu, Synchronously improved electromagnetic interference shielding and thermal conductivity for epoxy nanocomposites by constructing 3D copper nanowires/thermally annealed graphene aerogel framework, *Composites Part A: Applied Science and Manufacturing*, 128 (2020) 105670.
- [2] J. Li, J.L. Chen, X.H. Tang, J.H. Cai, J.H. Liu, M. Wang, Constructing nanopores in poly(oxymethylene)/multi-wall carbon nanotube nanocomposites via poly(l-lactide) assisting for improving electromagnetic interference shielding, *Journal of Colloid and Interface Science*, 565 (2020) 536-545.
- [3] A. Hazarika, B.K. Deka, D. Kim, H.E. Jeong, Y.B. Park, H.W. Park, Woven Kevlar Fiber/Polydimethylsiloxane/Reduced Graphene Oxide Composite-Based Personal Thermal Management with Freestanding Cu–Ni Core–Shell Nanowires, *Nano Letters*, 18 (2018) 6731-6739.
- [4] F. Shahzad, M. Alhabeab, C.B. Hatter, B. Anasori, S. Man Hong, C.M. Koo, Y. Gogotsi, Electromagnetic interference shielding with 2D transition metal carbides

- (MXenes), *Science*, 353 (2016) 1137-1140.
- [5] W.-C. Yu, T. Wang, Y.-H. Liu, Z.-G. Wang, L. Xu, J.-H. Tang, K. Dai, H.-J. Duan, J.-Z. Xu, Z.-M. Li, Superior and highly absorbed electromagnetic interference shielding performance achieved by designing the reflection-absorption-integrated shielding compartment with conductive wall and lossy core, *Chemical Engineering Journal*, 393 (2020) 124644.
- [6] T.-T. Li, Y. Wang, H.-K. Peng, X. Zhang, B.-C. Shiu, J.-H. Lin, C.-W. Lou, Lightweight, flexible and superhydrophobic composite nanofiber films inspired by nacre for highly electromagnetic interference shielding, *Composites Part A: Applied Science and Manufacturing*, 128 (2020) 105685.
- [7] W. Chen, L.-X. Liu, H.-B. Zhang, Z.-Z. Yu, Kirigami-Inspired Highly Stretchable, Conductive, and Hierarchical Ti₃C₂T_x MXene Films for Efficient Electromagnetic Interference Shielding and Pressure Sensing, *ACS nano*, (2021).
- [8] L.X. Liu, W. Chen, H.B. Zhang, Q.W. Wang, F.L. Guan, Z.Z. Yu, Flexible and Multifunctional Silk Textiles with Biomimetic Leaf-Like MXene/Silver Nanowire Nanostructures for Electromagnetic Interference Shielding, Humidity Monitoring, and Self-Derived Hydrophobicity, *Advanced Functional Materials*, 29 (2019) 1905197.
- [9] Y. Zhou, Z. Sun, L. Jiang, S. Chen, J. Ma, F. Zhou, Flexible and conductive meta-aramid fiber paper with high thermal and chemical stability for electromagnetic interference shielding, *Applied Surface Science*, 533 (2020) 147431.
- [10] Y. Zhou, Z. Sun, L. Jiang, S. Chen, J. Ma, F. Zhou, Highly Conductive Silver Nanoparticle-Functionalized Aramid Fiber Paper for Electrical Heaters with Rapid Response and Chemical Stability, *Industrial & Engineering Chemistry Research*, 59 (2020) 18898-18906.
- [11] L. Wang, X. Huang, D. Wang, W. Zhang, S. Gao, J. Luo, Z. Guo, H. Xue, J. Gao, Lotus leaf inspired superhydrophobic rubber composites for temperature stable piezoresistive sensors with ultrahigh compressibility and linear working range, *Chemical Engineering Journal*, 405 (2021) 127025.
- [12] B. Zhou, Z. Liu, C. Li, M. Liu, L. Jiang, Y. Zhou, F.-L. Zhou, S. Chen, S. Jerrams, J. Yu, A Highly Stretchable and Sensitive Strain Sensor Based on Dopamine Modified Electrospun SEBS Fibers and MWCNTs with Carboxylation, *Advanced Electronic Materials*, (2021) 2100233.
- [13] Y. Zhan, J. Wang, K. Zhang, Y. Li, Y. Meng, N. Yan, W. Wei, F. Peng, H. Xia, Fabrication of a flexible electromagnetic interference shielding Fe₃O₄@reduced graphene oxide/natural rubber composite with segregated network, *Chemical Engineering Journal*, 344 (2018) 184-193.
- [14] W.T. Cao, F.F. Chen, Y.J. Zhu, Y.G. Zhang, Y.Y. Jiang, M.G. Ma, F. Chen, Binary Strengthening and Toughening of MXene/Cellulose Nanofiber Composite Paper with Nacre-Inspired Structure and Superior Electromagnetic Interference Shielding Properties, *ACS Nano*, 12 (2018) 4583-4593.
- [15] J.C. Luo, S.J. Gao, H. Luo, L. Wang, X.W. Huang, Z. Guo, X.J. Lai, L.W. Lin, R.K.Y. Li, J.F. Gao, Superhydrophobic and breathable smart MXene-based textile for multifunctional wearable sensing electronics, *Chemical Engineering Journal*, 406 (2021)

- [16] J. Huang, M. Zhao, Y. Hao, D. Li, J. Feng, F. Huang, Q. Wei, Flexible, Stretchable, and Multifunctional Electrospun Polyurethane Mats with 0D-1D-2D Ternary Nanocomposite-Based Conductive Networks, 7 (2021) 2000840.
- [17] B. Hwang, A. Lund, Y. Tian, S. Darabi, C. Muller, Machine-Washable Conductive Silk Yarns with a Composite Coating of Ag Nanowires and PEDOT:PSS, *Acs Applied Materials & Interfaces*, 12 (2020) 27537-27544.
- [18] K.H. Pyo, J.W. Kim, Transparent and mechanically robust flexible heater based on compositing of Ag nanowires and conductive polymer, *Composites Science and Technology*, 133 (2016) 7-14.
- [19] S. Sung, T.W. Kim, Flexible nonvolatile memory devices based on Au/PMMA nanocomposites deposited on PEDOT:PSS/Ag nanowire hybrid electrodes, *Applied Surface Science*, 411 (2017) 67-72.
- [20] C. Liang, K. Ruan, Y. Zhang, J. Gu, Multifunctional Flexible Electromagnetic Interference Shielding Silver Nanowires/Cellulose Films with Excellent Thermal Management and Joule Heating Performances, *ACS Applied Materials & Interfaces*, 12 (2020) 18023-18031.
- [21] H. Hu, S. Wang, S. Wang, G. Liu, T. Cao, Y. Long, Aligned Silver Nanowires Enabled Highly Stretchable and Transparent Electrodes with Unusual Conductive Property, *Advanced Functional Materials*, 29 (2019) 1902922.
- [22] A. Kim, J. Ahn, H. Hwang, E. Lee, J. Moon, A pre-strain strategy for developing a highly stretchable and foldable one-dimensional conductive cord based on a Ag nanowire network, *Nanoscale*, 9 (2017) 5773-5778.
- [23] S. Chen, L. Song, Z. Tao, X. Shao, Y. Huang, Q. Cui, X. Guo, Neutral-pH PEDOT:PSS as over-coating layer for stable silver nanowire flexible transparent conductive films, *Organic Electronics*, 15 (2014) 3654-3659.
- [24] Y. Zhao, X. Wang, S. Yang, E. Kuttner, A.A. Taylor, R. Salemmilani, X. Liu, M. Moskovits, B. Wu, A. Dehestani, J.-F. Li, M.F. Chisholm, Z.-Q. Tian, F.-R. Fan, J. Jiang, G.D. Stucky, Protecting the Nanoscale Properties of Ag Nanowires with a Solution-Grown SnO₂ Monolayer as Corrosion Inhibitor, *Journal of the American Chemical Society*, 141 (2019) 13977-13986.
- [25] J. Luo, L. Huo, L. Wang, X. Huang, J. Li, Z. Guo, Q. Gao, M. Hu, H. Xue, J. Gao, Superhydrophobic and multi-responsive fabric composite with excellent electro-photo-thermal effect and electromagnetic interference shielding performance, *Chemical Engineering Journal*, 391 (2020) 123537.
- [26] Y. Wang, F.-q. Gu, L.-j. Ni, K. Liang, K. Marcus, S.-l. Liu, F. Yang, J.-j. Chen, Z.-s. Feng, Easily fabricated and lightweight PPy/PDA/AgNW composites for excellent electromagnetic interference shielding, *Nanoscale*, 9 (2017) 18318-18325.
- [27] Y. Wang, W. Wang, X.D. Ding, D. Yu, Multilayer-structured Ni-Co-Fe-P/polyaniline/polyimide composite fabric for robust electromagnetic shielding with low reflection characteristic, *Chemical Engineering Journal*, 380 (2020) 11.
- [28] S. Ghosh, S. Ganguly, S. Remanan, N.C. Das, Fabrication and investigation of 3D tuned PEG/PEDOT: PSS treated conductive and durable cotton fabric for superior electrical conductivity and flexible electromagnetic interference shielding, *Composites Science and Technology*, 181 (2019) 107682.

- [29] Y.-F. Wang, T. Sekine, Y. Takeda, K. Yokosawa, H. Matsui, D. Kumaki, T. Shiba, T. Nishikawa, S. Tokito, Fully Printed PEDOT:PSS-based Temperature Sensor with High Humidity Stability for Wireless Healthcare Monitoring, *Scientific reports*, 10 (2020) 2467.
- [30] Y.J. Tan, J. Li, Y. Gao, J. Li, S.Y. Guo, M. Wang, A facile approach to fabricating silver-coated cotton fiber non-woven fabrics for ultrahigh electromagnetic interference shielding, *Applied Surface Science*, 458 (2018) 236-244.
- [31] J. Gao, J. Luo, L. Wang, X. Huang, H. Wang, X. Song, M. Hu, L.C. Tang, H. Xue, Flexible, superhydrophobic and highly conductive composite based on non-woven polypropylene fabric for electromagnetic interference shielding, *Chemical Engineering Journal*, 364 (2019) 493-502.
- [32] Y.N. Gao, Y. Wang, T.N. Yue, Y.X. Weng, M. Wang, Multifunctional cotton non-woven fabrics coated with silver nanoparticles and polymers for antibacterial, superhydrophobic and high performance microwave shielding, *Journal of Colloid and Interface Science*, 582 (2021) 112-123.
- [33] M.H. Al-Saleh, W.H. Saadeh, U. Sundararaj, EMI shielding effectiveness of carbon based nanostructured polymeric materials: A comparative study, *Carbon*, 60 (2013) 146-156.
- [34] W. Wang, R. Li, M. Tian, L. Liu, H. Zou, X. Zhao, L. Zhang, Surface Silverized Meta-Aramid Fibers Prepared by Bio-inspired Poly(dopamine) Functionalization, *ACS Applied Materials & Interfaces*, 5 (2013) 2062-2069.
- [35] I.K. Moon, S. Yoon, J. Oh, 3D Highly Conductive Silver Nanowire@PEDOT:PSS Composite Sponges for Flexible Conductors and Their All-Solid-State Supercapacitor Applications, 4 (2017) 1700860.
- [36] Y. Ding, W. Xu, W. Wang, H. Fong, Z. Zhu, Scalable and Facile Preparation of Highly Stretchable Electrospun PEDOT:PSS@PU Fibrous Nonwovens toward Wearable Conductive Textile Applications, *ACS Applied Materials & Interfaces*, 9 (2017) 30014-30023.
- [37] N.M. Nair, J.K. Pakkathillam, K. Kumar, K. Arunachalam, D. Ray, P. Swaminathan, Printable Silver Nanowire and PEDOT:PSS Nanocomposite Ink for Flexible Transparent Conducting Applications, *Acs Applied Electronic Materials*, 2 (2020) 1000-1010.
- [38] Z. Ma, S. Kang, J. Ma, L. Shao, Y. Zhang, C. Liu, A. Wei, X. Xiang, L. Wei, J. Gu, Ultraflexible and Mechanically Strong Double-Layered Aramid Nanofiber-Ti₃C₂T_x MXene/Silver Nanowire Nanocomposite Papers for High-Performance Electromagnetic Interference Shielding, *ACS Nano*, 14 (2020) 8368-8382.
- [39] A.K. Singh, A. Shishkin, T. Koppel, N. Gupta, A review of porous lightweight composite materials for electromagnetic interference shielding, *Composites Part B: Engineering*, 149 (2018) 188-197.
- [40] H. Jia, X. Yang, Q.-Q. Kong, L.-J. Xie, Q.-G. Guo, G. Song, L.-L. Liang, J.-P. Chen, Y. Li, C.-M. Chen, Free-standing, anti-corrosion, super flexible graphene oxide/silver nanowire thin films for ultra-wideband electromagnetic interference shielding, *Journal of Materials Chemistry A*, 9 (2021) 1180-1191.
- [41] L. Lu, D. Xing, K.S. Teh, H. Liu, Y. Xie, X. Liu, Y. Tang, Structural effects in a

composite nonwoven fabric on EMI shielding, *Materials & Design*, 120 (2017) 354-362.

[42] J. Luo, L. Wang, X. Huang, B. Li, Z. Guo, X. Song, L. Lin, L. Tang, H. Xue, J. Gao, Mechanically Durable, Highly Conductive, and Anticorrosive Composite Fabrics with Excellent Self-Cleaning Performance for High-Efficiency Electromagnetic Interference Shielding, *ACS Applied Materials & Interfaces*, 11 (2019) 10883-10894.

[43] Z. Zhan, Q. Song, Z. Zhou, C. Lu, Ultrastrong and conductive MXene/cellulose nanofiber films enhanced by hierarchical nano-architecture and interfacial interaction for flexible electromagnetic interference shielding, *Journal of Materials Chemistry C*, 7 (2019) 9820-9829.

[44] L.C. Jia, L. Xu, F. Ren, P.G. Ren, D.X. Yan, Z.M. Li, Stretchable and durable conductive fabric for ultrahigh performance electromagnetic interference shielding, *Carbon*, 144 (2019) 101-108.

[45] J. Ma, M. Zhan, K. Wang, Ultralightweight Silver Nanowires Hybrid Polyimide Composite Foams for High-Performance Electromagnetic Interference Shielding, *ACS Applied Materials & Interfaces*, 7 (2015) 563-576.

[46] N. Kim, S. Kee, S.H. Lee, B.H. Lee, Y.H. Kahng, Y.-R. Jo, B.-J. Kim, K. Lee, Highly Conductive PEDOT:PSS Nanofibrils Induced by Solution-Processed Crystallization, *Adv. Mater.*, 26 (2014) 2268-2272.

[47] Q.W. Wang, H.B. Zhang, J. Liu, S. Zhao, X. Xie, L. Liu, R. Yang, N. Koratkar, Z.Z. Yu, Multifunctional and Water-Resistant MXene-Decorated Polyester Textiles with Outstanding Electromagnetic Interference Shielding and Joule Heating Performances, *Advanced Functional Materials*, 29 (2019) 1806819.

[48] I.K. Moon, J.I. Kim, H. Lee, K. Hur, W.C. Kim, H. Lee, 2D Graphene Oxide Nanosheets as an Adhesive Over-Coating Layer for Flexible Transparent Conductive Electrodes, *Scientific Reports*, 3 (2013) 1112.

[49] Z. Ma, S. Kang, J. Ma, L. Shao, A. Wei, C. Liang, J. Gu, B. Yang, D. Dong, L. Wei, Z. Ji, High-Performance and Rapid-Response Electrical Heaters Based on Ultraflexible, Heat-Resistant, and Mechanically Strong Aramid Nanofiber/Ag Nanowire Nanocomposite Papers, *ACS Nano*, 13 (2019) 7578-7590.

[50] R. Zhou, P. Li, Z. Fan, D. Du, J. Ouyang, Stretchable heaters with composites of an intrinsically conductive polymer, reduced graphene oxide and an elastomer for wearable thermotherapy, *Journal of Materials Chemistry C*, 5 (2017) 1544-1551.